MECHANICAL PROPERTIES AND CONSTRUCTION OF CONSTITUTIVE MODEL FOR COMPRESSION AND STRESS RELAXATION OF CATTLE MANURE

/

牛粪压缩和应力松弛特性及其本构模型构建研究

Weisong ZHAO[1,2), Yongsheng CHEN[1,2), Weiqiang LIN[3), Zhenwei WANG[1,2), Qimin GAO[1), Hu XIE[1),
Biao MA[1), Mingjiang CHEN[*1), Jingjing FU[*1,2)

[1) Nanjing Institute of Agricultural Mechanization, Ministry of Agriculture and Rural Affairs, Nanjing 210014, China;
[2) Western Research Institute, CAAS, Changji 831100, China;
[3) Zhongnong Guoke (Nanjing) Planning and Design Co., Ltd，Nanjing 210014, China;
Tel: +86 02584346161; E-mail: chenmingjiang@caas.cn; tutujing12@163.com
Correspondent authors: Mingjiang Chen, Jingjing Fu

ABSTRACT

In order to study the mechanical properties of compression and stress relaxation of manure under drainage conditions, the experiment was carried out with cattle manure as the object, and the constitutive models were improved to describe the stress-strain curves of compression and stress relaxation. The defined constitutive model was determined by parameter identification, and the influence laws of moisture content and filling mass on the compression and relaxation process were investigated. The results show that the improved Nishihara model and the five-component generalized Maxwell model can better describe the compression and stress relaxation properties of cattle manure, and the coefficients of determination of the parameters of the fitted intrinsic model are all greater than 0.9, with high fitting accuracy. The compression process was divided into three stages: exhaust, drainage, and viscoelastic-plastic deformation. The stress decay rate tended to change quickly and then slowly, and there was a negative correlation between the compressed mass, moisture content, and stress decay rate. Duncan's mean comparisons revealed that the differences in elastic modulus between different moisture content / compressed mass groups in the parameters of the cattle manure compression principal model were all significant (P<0.05). The differences in elastic modulus and coefficient of viscous attenuation between different moisture content groups in the parameters of the stress relaxation model were all significant. The study's results can provide the theoretical basis for the study and simulation of CM's compression and dewatering mechanism and provide support for the solid-liquid separator for livestock and poultry manure.

摘要

压缩过程中粪污的力学特性尚不清晰，严重制约固液分离机具的优化改进。为研究排水条件下牛粪压缩及应力松弛的力学特性，以牛粪为对象开展试验，分别采用改进西原模型和五元件广义 Maxwell 模型对压缩和应力松弛的应力应变曲线进行描述。通过定义的本构模型对不同含水率、压缩质量的牛粪力学试验数据进行参数辨识，确定相关模型参数，并探究各因素对压缩及松弛过程的影响规律。研究结果表明：改进西原模型、五元件广义 Maxwell 模型可以较好地描述牛粪压缩、应力松弛特性，拟合求解的本构模型参数决定系数均大于 0.9，拟合精度高。压缩过程分为排气、排水和粘弹塑性变形 3 个阶段；应力衰减速率呈先快后慢变化趋势，压缩质量、含水率与应力衰减速度呈负相关关系。Duncan 均值比较结果发现：牛粪压缩本构模型参数中不同含水率/压缩质量组间弹性模量差异均显著（P<0.05）；应力松弛模型参数中不同含水率组间弹性模量和粘性衰减系数差异均显著（P<0.05）。压缩与应力松弛力学特性的研究结果可为牛粪压缩脱水机理研究、仿真模拟提供理论依据，为畜禽粪便固液分离机具提供支撑。

INTRODUCTION

The annual production of livestock manure in China is 4 billion tons (*Wang et al., 2023*; *Yi et al., 2021*), which is vast. In China, the direct discharge of untreated livestock manure is prohibited, and the government encourages the utilization of livestock manure as a resource to achieve sustainable development of animal husbandry (*Bai et al., 2016*). The moisture content of livestock and poultry manure is generally above 80%, and solid-liquid separation (compression dehydration) is the critical common link in the pre-treatment of comprehensive utilization of manure (*Cârdei P. et al., 2019*; *Hjorth et al., 2010*).

After solid-liquid separation, dry solids and low-impurity liquids are obtained, facilitating subsequent management, disposal, and return to the field, reducing the cost of manure treatment and greenhouse gas emissions from farms (*Aguirre-Villegas et al.*, *2019*; *Guilayn et al.*, *2019*; *Husfeldt et al.*, *2012*). Currently, screw press or press auger is widely used in solid-liquid separation of livestock manure *(Guan et al., 2016; Zhao et al., 2017)*. The machine mainly comprises a motor, screw, screen, and other components. In a screw press separator, the effluent is transported into a cylindrical screen with a screw. The liquid will pass through the screen and be collected. At the end of the axle, the DM-rich fraction will be pressed against the plate, and more liquid will be pressed out of the solid fraction. The solid phase will drop from the opening between the plate and the opening of the cylindrical mesh (*Stefan et al.*, *2021*; *Stefan et al.*, *2019*; *Zhao et al., 2017*). With the attenuation of water content, the dewatering of livestock and poultry manure produces a phase change process from liquid to solid, and the body change process further compresses the cake (solid). In the later stage of dewatering, the manure particles are deformed and rebound due to extrusion and friction, which makes the machine generally have the problems of high energy consumption, unstable operation performance (high or low moisture content of solids after dewatering), and mutual inhibition of processing efficiency and dewatering degree. In order to achieve the screw press dewatering, both presses dry and squeeze fast operating effect, the group designed a broken tooth screw, through the manure stress increase, release, and then increase, to achieve the principle of nonlinear compression dewatering of the alternating load, and experimental and simulation research (*Zhu et al., 2017*).

Livestock manure compression dewatering from the highly abstracted model point of view can be understood as the role of the external load (effective stress), the pore water between the manure particles through the porous media discharge, manure particles skeleton acts as a spring to produce deformation. However, the modulus of this "spring" will change with the change of effective stress, and the degree and speed of deformation are mainly related to the compression mode and the nature of fecal matter itself. In recent years, scholars have measured fecal matter's particle size distribution and nutrient content, studied fecal matter's rheological properties, and clarified the critical value of fecal matter as a Newtonian and non-Newtonian fluid (*Shi et al., 2014; Ehlers et al.*, *2012*). However, the manure's compression and stress relaxation characteristics under loading are not precise, and the constitutive model has yet to be established.

Therefore, the compression mechanical properties test is carried out in this study with cattle manure (CM) as the research object, and the compression and stress relaxation tests are carried out using a universal testing machine with the moisture content (MC) and filling mass (LM) as the test factors. The obtained stress-strain data were curve-fitted, the parameters of the defined constitutive model were identified, and then the compression mechanical properties of CM were studied. The results may provide theoretical information for studying manure compression and dewatering mechanism, simulation, and optimization design of solid-liquid separators.

MATERIALS AND METHODS
Test materials and equipment
Manure sample preparation

The manure used in the experiment was obtained from Hexing Dairy Farm, Haimen District, Jiangsu Province, China. The 9GY-16B Livestock Manure Solid-Liquid Separator developed by the Nanjing Institute of Agricultural Mechanization, Ministry of Agriculture and Rural Affairs, was used to separate fresh cow manure to obtain cow manure solids with a moisture content of about 70%. The moisture content of CM was regulated by the natural drying method and the addition of deionized water, and CM with a moisture content of 50%, 65%, and 80% were obtained and sealed in plastic boxes. The compression vessel was 252 mm in height, 108 mm in outer diameter, and 2 mm in wall thickness, made of 304 stainless steel, with small holes (2 mm in diameter) around the cylinder wall for drainage. Sequentially, 500 g, 750 g, and 1000 g of CM with 50%, 65%, and 80% moisture content were placed into the compression vessel with a pre-pressure of 5 N. The test samples with different moisture contents were numbered by filling in the mass-test number. Each set of tests was repeated three times, and 27 test samples were prepared.

Compression and stress relaxation test equipment and methods

The test equipment used is Jinan Chuanbai Instrument and Equipment Co., Ltd., production of a microcomputer-controlled electronic universal testing machine and self-made compression device, universal testing machine model WDW-20, grade 0.5 level. Self-made compression device including pressure rod, compression container, acrylic shell, faucet and base, and other components.

Other auxiliary instruments include the DGH30-1A electric heating blast drying oven produced by Nanjing Testing Instrument Factory and the YP300001D electronic scale (range 0-30 kg, accuracy 0.1g) produced by Shanghai Lichen Instrument Technology Co.

CM was considered a whole in the compression process, and the compression cross-sectional area and initial height were entered into the universal testing machine. Through the program control module, the movement speed of the compression bar is set to 50 mm/min, and the compression is stopped when the stress reaches 0.8 MPa. The computer software will measure the load value and deformation and transform them to get the stress-strain (compression) curve. After each group of compression tests stops loading, the compression rod does not move to keep the deformation of fecal matter, and the value of stress change is recorded by the universal testing machine. The test is ended after 120 seconds to get the change curve of stress with time (stress relaxation curve). The compression displacement and drainage mass when the compression stress reached the maximum value were recorded during the test.
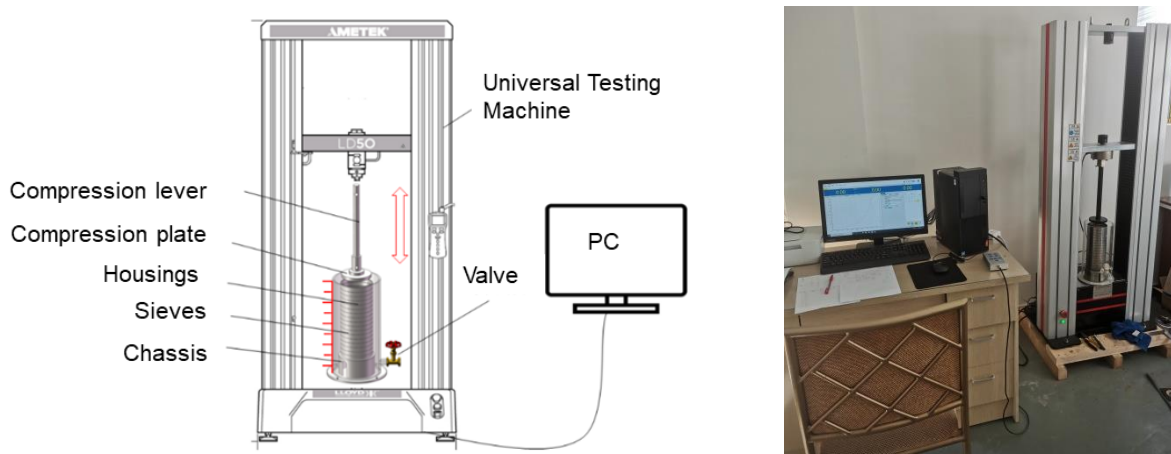
Fig. 1 - Compression test device

Methods of constructing the intrinsic model and determining the parameters of the intrinsic equations

Firstly, the stress-strain curves and stress-relaxation curves during compression of CM were obtained experimentally to study the compression and relaxation characteristics; secondly, the compression and stress-relaxation models of CM were constructed concerning the research methods of the previous researchers on related materials (e.g., soil, straw, seed cotton, etc.) (*Ding et al., 2023; Wang et al., 2021; Kong et al., 2021; Nona et al.*, *2014*). Then, series-parallel arithmetic rules were applied to solve the constitutive equations, and the experimental values were used as the target to test the difference between the calculated values obtained by the constitutive equation and the experimental values so that the proper constitutive model and equations could be determined; lastly, the parameter values of the constitutive equations corresponding to all the experiments were obtained by using the 1stOpt and Matlab software to solve the equations.

RESULTS
Analysis of compression test

The compression curves of 500, 750, and 1000 g FM at 50%, 65%, and 80% MC with a loading speed of 50 mm/min are shown in Fig. 2. As can be seen from Fig. 2, the characteristics of the stress-strain curves obtained from each group of repeated tests were the same, and the dispersion was not significant. Under different MC, the compression stress-strain curve of CM has the same trend. With the increase of strain, the stress shows a slow and then fast growth trend. The compactness of CM increased with the rise of stress, and the bulk modulus increased, indicating that the CM has compression hardness. However, it was also observed that MC and FM have an effect on the rate of change of the stress-strain curve. For example, for the same MC and strain conditions, the higher the FM, the higher the stress value of CM, and the difference in stress gradually increases with the decrease of MC. This indicated that CM has compression hardness (Yao et al., 2023), and the lower the MC, the better the compression hardness; the increase of MC will reduce the sensitivity of the FM to the stress-strain.
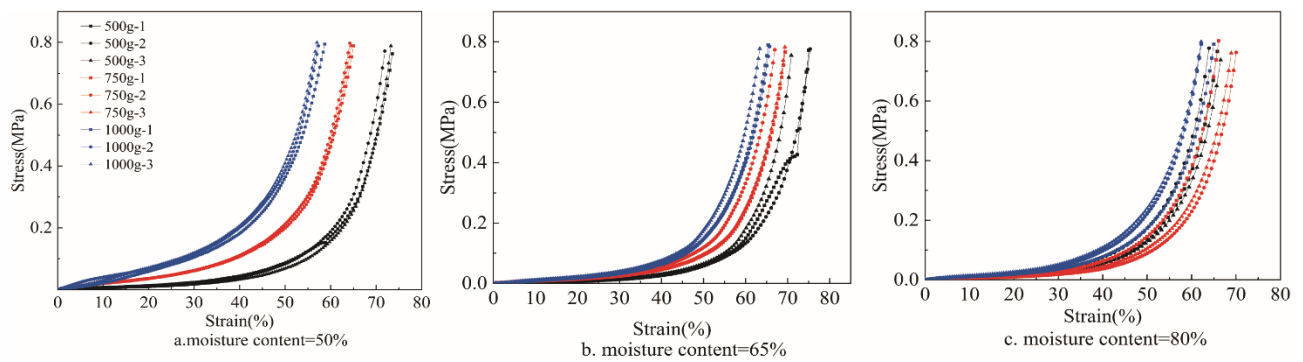
Fig. 2 - Compression stress-strain curve of CM with different MC

The mechanical changes of CM in the compression and dehydration process are more complicated, mainly manifested in viscoelastic properties. Through the observation of the test process and the analysis of the compression curve (Fig. 2), it is found that the stress growth rate in the initial stage of compression is slow. The curve is flat, probably because this stage is mainly exhausting, and the CM particles undergo misalignment and rearranging, which will be referred to as the exhausting stage. As compression proceeds, the growth rate of stress becomes faster, and the particles and moisture are compressed as the load-bearing body in this stage, which is drainage-based. Direct contact, slip, and deformation between particles occur, and this stage is called the drainage stage. After that, the stress increases significantly with the increase of strain, and this stage is mainly compressed CM particles, accompanied by a small amount of moisture overflow. The particle volume decreases significantly, the density increases and the particles undergo elastic or plastic deformation; this stage is the visco-elastic-plastic deformation stage.

Analysis of typical compression stress-strain curves of CM revealed that it showed prominent elastic characteristics in the initial and later stages of compression (Fig. 3), and the reason for this was analyzed to be probably related to the moisture content. In the venting stage, the stress change is small (0 to 0.04 MPa) in the extensive strain range (0 to 40%), and the curve as a whole is quasi-linear; in the draining stage (stress from 0.04 to 0.3 MPa), probably due to the fast draining speed and large draining volume of CM, the CM particles begin to deform plastically, and thus the modulus increases gradually; and in the late stage of dewatering (stress >0.3 MPa), there is only a tiny amount of moisture discharged In the late stage of dewatering (stress > 0.3 MPa), only a little water was discharged, and the moisture content of CM was in a relatively stable state. Although the stress increased exponentially, the stress-to-strain ratio was stable, indicating that CM had good elasticity characteristics at this stage.
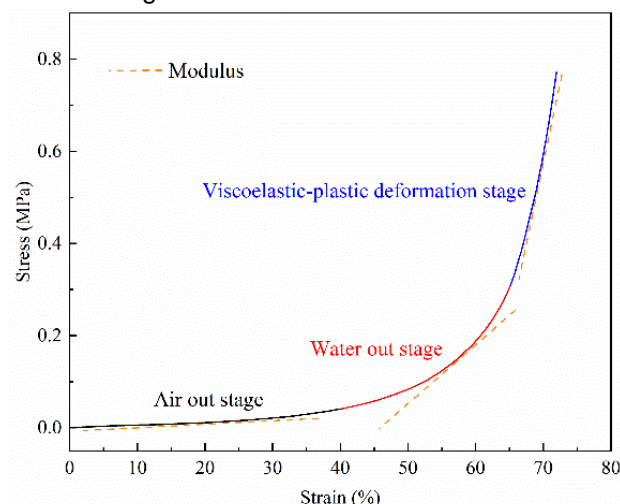
Fig. 3 - Typical stress response of the compression experiment

Analysis of stress relaxation tests

Figure 4 demonstrates the stress relaxation curves of CM with 500, 750, and 1000g FM at 50%, 65%, and 80% MC. It can be seen that the characteristics of the curves obtained from each group of repeated tests are the same, i.e., the rate of stress attenuation shows a tendency to change quickly and then slowly and finally tends to be stabilized, which is similar to the relaxation characteristics of agricultural materials, such as cotton and straw (*Kong et al., 2021; Ma et al., 2016*).
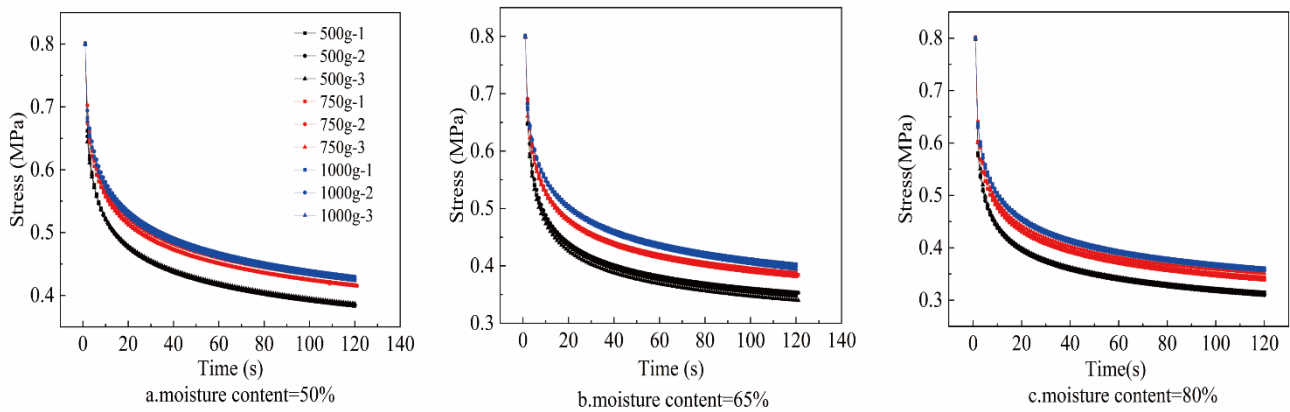
Fig. 4 - Stress relaxation curve of CM with different MC

Figure 4 shows that at the exact moment, the smaller the FM, the smaller the stress, indicating that the FM negatively correlates with the stress decay rate. In order to further observe the effect of MC on stress relaxation, the stress relaxation curves under 50%, 65%, and 80% MC are plotted with 750g FM for example (Fig. 5). Fig. 5 shows that at the same time, the greater the MC, the smaller the stress; the time required for the stress to decay from 0.8 MPa to 0.6 MPa (attenuation ratio is 25%) under 50%, 65%, and 80% MC corresponds to 6, 4, and 2 s, indicating a negative correlation between MC and stress decay rate. The reason may be that under the same FM, the higher the MC, the less the dry matter of CM, the smaller the particle contact surface, and the larger the pores, so the stress dissipation speed is faster after being compressed.
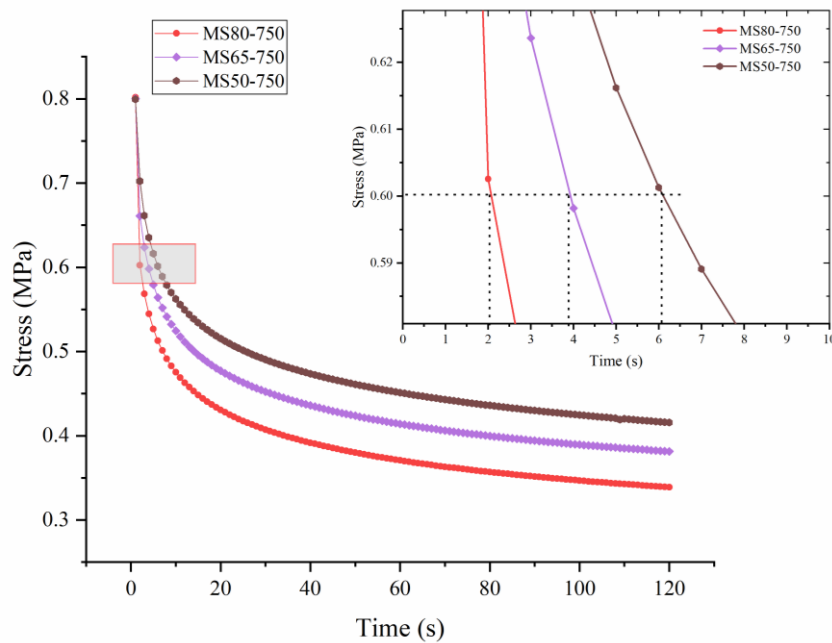
Fig. 5 - Effect of MC on the stress decay rate

Model Construction
Compression principal model

The Nishihara body model (*You W. et al., 2022*) (Fig.6a), which is composed of Hooke, Kelvin and viscoplastic bodies in series, is suitable for reflecting the compressive mechanical properties of soft materials, but it describes stage 1 as elasticity only. The intrinsic equations of the Westphalian body are:

$$\begin{cases} \frac{\eta_1}{E_1}\dot{\sigma} + \left(1 + \frac{E_2}{E_1}\right)\sigma = \eta_1\dot{\varepsilon} + E_2\varepsilon\,(\sigma < \sigma_f) \\ \ddot{\sigma} + \left(\frac{E_2}{\eta_1} + \frac{E_2}{\eta_2} + \frac{E_1}{\eta_1}\right)\dot{\sigma} + \frac{E_1E_2}{\eta_1\eta_2}(\sigma - \sigma_f) = E_2\ddot{\varepsilon} + \frac{E_1E_2}{\eta_1}\dot{\varepsilon}\,(\sigma \geq \sigma_f) \end{cases} \tag{1}$$

where σ is the total stress, MPa; $\dot{\sigma}, \ddot{\sigma}$ are the first and second order derivatives of the total stress with respect to time, respectively; $\dot{\varepsilon}, \ddot{\varepsilon}$ are the first and second order derivatives of the total strain with respect to time, respectively; E_1, E_2 are the elastic moduli of the Hooke body in the Hooker body element and the Kelvin body

element, MPa, respectively; η_1, η_2 are the viscous modulus of the Newtonian body in the Kelvin element and the visco-plastic body, MPa-s; σ_f is the initial stress of the Coulomb body in the visco-plastic body, MPa.

In order to better reflect the viscoelastic properties of the material, Fanting Kong et al. (*Kong. et al., 2021*) added one Newtonian body to obtain a modified Westfield body (Fig. 6b), established a model that uniformly reflects the three compression stages, and applied the tandem operation rule to derive the intrinsic equation of the modified Westfield body model, as shown in Eq. 2.

a. Nishihara model   b. Improved Nishihara model
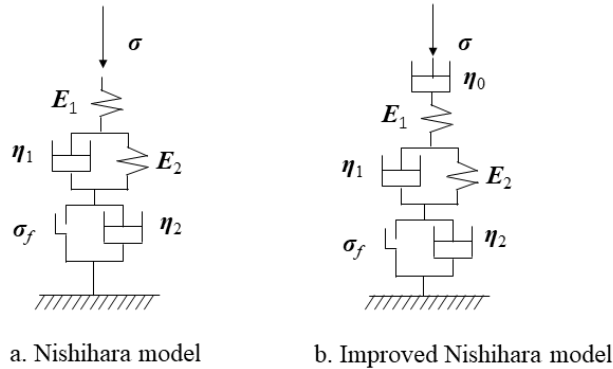
Fig. 6 - Compression mechanical model

σ is total stress, MPa; η_1 is viscosity modulus of tandem Newtonian body, MPa·s; E_1 is elasticity modulus of tandem Hookean body, MPa; E_2 is elasticity modulus of Hookean body in Kelvin body, MPa; η_2 is viscosity modulus of Newtonian body in Kelvin body, MPa·s; σ_f is initial stress of Cullen body, MPa; η_3 is viscosity modulus of Newtonian body in Viscoplastic body, MPa·s.

$$\begin{cases} \frac{\eta_1}{E_2}\ddot{\sigma} + \left(1 + \frac{E_2}{E_1} + \frac{\eta_1}{\eta_0}\right)\dot{\sigma} + \frac{E_2}{\eta_0}\sigma = \eta_1\ddot{\varepsilon} + E_2\dot{\varepsilon} & (\sigma < \sigma_f) \\ \frac{\eta_1}{E_1}\ddot{\sigma} + \left(1 + \frac{\eta_1}{\eta_2} + \frac{E_2}{E_1} + \frac{\eta_1}{\eta_0}\right)\dot{\sigma} + \left(\frac{E_2}{\eta_0} + \frac{E_2}{\eta_2}\right)\sigma - \frac{E_2}{\eta_2}\sigma_f = \eta_1\ddot{\varepsilon} + E_2\dot{\varepsilon} & (\sigma \geq \sigma_f) \end{cases} \tag{2}$$

The compression process of CM is constant velocity compression, so the first order derivative of strain with respect to time is constant and the second order derivative is zero, i.e., $\dot{\varepsilon}=$ constant and $\ddot{\varepsilon}= 0$. Collating Eq. (2) yields the intrinsic equations of the visco-elastic-plastic model of CM compression as:

$$\begin{cases} \frac{\eta_1}{E_2}\ddot{\sigma} + \left(1 + \frac{E_2}{E_1} + \frac{\eta_1}{\eta_0}\right)\dot{\sigma} + \frac{E_2}{\eta_0}\sigma = C_1 & (\sigma < \sigma_f) \\ \frac{\eta_1}{E_1}\ddot{\sigma} + \left(1 + \frac{\eta_1}{\eta_2} + \frac{E_2}{E_1} + \frac{\eta_1}{\eta_0}\right)\dot{\sigma} + \left(\frac{E_2}{\eta_0} + \frac{E_2}{\eta_2}\right)\sigma - \frac{E_2}{\eta_2}\sigma_f = C_2 & (\sigma \geq \sigma_f) \end{cases} \tag{3}$$

With MC as 65%, the data of the first repeated test of 500 g FM were fitted, and the fitting effect is shown in Fig. 7. From the fitting curve, it can be seen that the coefficient of determination R^2 of the fit result of the Nishihara model is 0.926, and the coefficient of determination R^2 of the fitting result of the optimized Nishihara model is 0.974. The fitting curve is basically consistent with the test curve, indicating the fitting accuracy. The higher the value, the more accurate the fitting result. Therefore, the optimized Nishihara model was chosen to construct the constitutive model of CM compression stage.
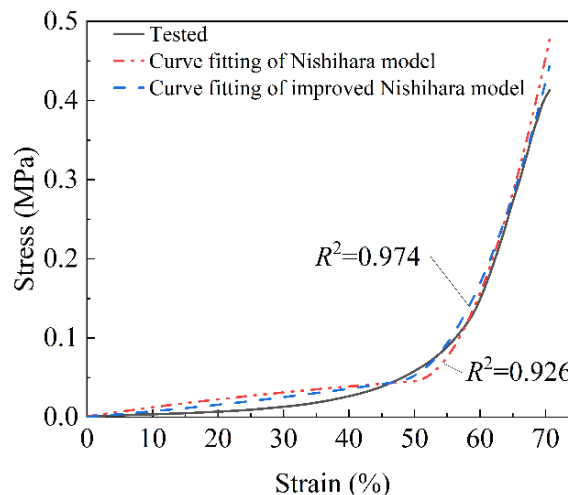
Fig. 7 - Curve fitting of compression model

Stress relaxation model

It can be seen from Fig. 4 that the stress relaxation curves of CM under different compression conditions have similar shapes and basically the same changing rules, so the same model can be used to describe them. Studies have shown that the stress relaxation characteristics are often described by the generalized Maxwell model, which can be divided into a three-element generalized Maxwell model (Fig. 8a) and a five-element generalized Maxwell model (Fig. 8b) according to the number of elements. The three-element generalized Maxwell model is composed of a Hooke element and a Maxwell model connected in parallel, and its stress relaxation stage equation is as follows:

$$\sigma(t) = \varepsilon_i\left(E_a e^{-t/T_a} + E_e\right) \tag{4}$$

In the formula $\sigma(t)$ is the stress at time t, MPa; ε_i is the initial strain; t is time, s; T_a is the stress relaxation time of Maxwell element $T_a = \eta_a/E_a$, s; η_a is the viscosity modulus of Newton body, MPa·s.

The five-element generalized Maxwell models is a Maxwell model connected in parallel in the three-element generalized Maxwell model, and its stress relaxation stage equation is:

$$\sigma(t) = \varepsilon_0\left(E_a e^{-t/T_a} + E_b e^{-t/T_b} + E_e\right) \tag{5}$$

where ε_0 is the initial strain, %; E_a, E_b are the damping elastic moduli of the first and second Maxwell bodies, MPa; T_a and T_b are the stress relaxation times of the first and second Maxwell bodies, $T_a = \eta_a/E_a$, $T_b = \eta_b/E_b$, s; η_a, η_b are the attenuation viscosity coefficients of the first and second Maxwell bodies, respectively, MPa·s ; E_e is the instantaneous elastic modulus, MPa.

a. Generalized Maxwell 3-element mechanical model

b. Generalized Maxwell 5-element mechanical model
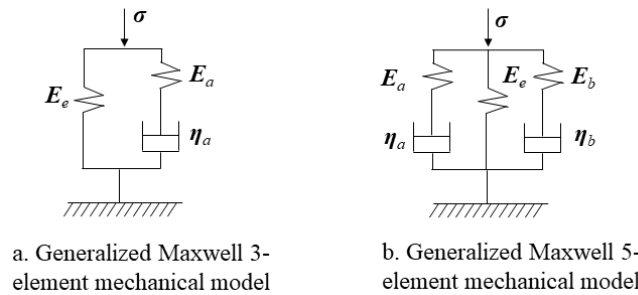
Fig. 8 - Stress relaxation mechanical model

E_e is instant elastic modulus; E_a and E_b are decaying elastic modulus of the first and second Maxwell body, respectively; η_a and η_b are decay viscosity coefficients of the first and second Maxwell body, respectively; σ is real-time stress.

It can be seen from Eq. (4) that the three-element generalized Maxwell model contains only one stress relaxation time T_a; it can be seen from Eq. (5) that the five-element generalized Maxwell model contains two stress relaxation times, T_a and T_b. It can be seen from Fig. 4 that the stress relaxation process of CM tends to be fast first and then slow, and the five-element generalized Maxwell model has more advantages. The data of the third repeated test with a MC of 65% and 1000 g FM were used for fitting, and the fitting effect is shown in Fig. 9.
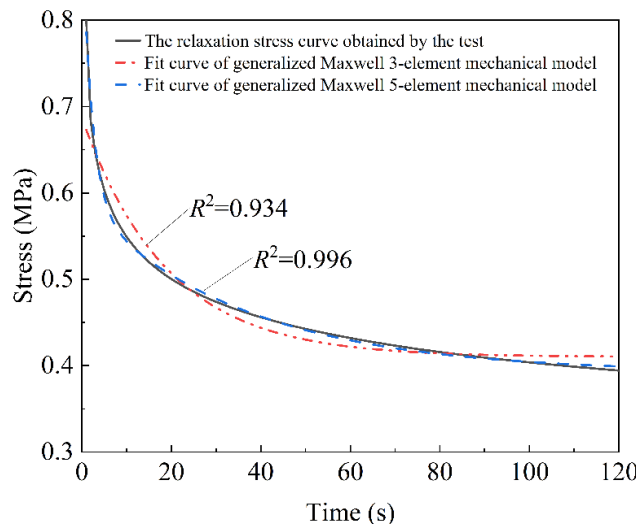
Fig. 9 - Fitting curve of stress relaxation model

The coefficient of determination R^2 of the fitting equation of the three-element generalized Maxwell model is 0.934, and the difference between the fitting curve and the test curve is large; the coefficient of determination of the fitting equation of the five-element generalized Maxwell model R^2 is 0.996, which indicates a high fitting accuracy. Therefore, the five-element generalized Maxwell model is chosen to construct the constitutive model in the relaxation stage.

Parameter determination and analysis
Parameter determination

The constitutive equation of the optimized Nishihara model was written into the 1stOpt software by programming, and the parameters of the compressive stress-strain curves of CM under the test conditions of 50%, 65%, 80% MC, and 500, 750, and 1000 g FM were respectively calculated. Fitting (a total of 27 groups) was solved to obtain six parameters to be determined in the constitutive equation, namely E_1, E_2, η_0, η_1, η_2, and σ_f. SPSS software was used to process the solved parameter values to obtain. The parameter values of the CM compressive model were compared and analyzed using the Duncan's mean multiple comparison method, and the results are shown in Table 1.

Table 1

Effects of moisture content and compression mass on the parameters of the CM compression constitutive model

	FM	E_1	E_2	η_0	η_1	η_2	σ_f	R^2
50%	500	112.7±12.64 aA	0.76±0.15a A	2.86E13±4.96E13 aA	4.42E4±3.12E3aB	2.90E14±5.02E14aA	0.11±0.01aA	0.93±0.03
	750	462±18.23a B	6.26±0.49 aA	4.09E12±7.07E9 aA	2.25E6±3.93E4aA	3.53E18±3.96E16aC	0.14±0.003bB	0.96±0.01
	1000	2203.33±115.47aC	49.03±13.05aB	2.18E13±5.77E11aA	1.26E8±1.16E7aB	4.59E16±1.01E16bB	0.17±0.003bC	0.94±0.03
65%	500	1.25E4±7.86E3bA	5.35E1±1.91E1bB	1.22E11±1.17E10aA	1.95E8±2.12E7bA	5.6E12±6.72E10aA	0.09±0.01aA	0.96±0.003
	750	2.41E7±2.26E6aB	6.99E1±3.55aC	2.69E17±5.47E16aB	1.93E12±2.31E11aB	5.24E15±1.65E15aB	0.04±0.03aA	0.928±0.03
	1000	2.20E5±2.31E4aA	3.48±0.29a A	2.96E10±1.09E9aA	8.35E8±2.88E7aA	1.92E11±1.99E10aA	0.08±0.03aA	0.94±0.01
80%	500	5.30E3±2.0E3abA	1.78E1±1.09E1aA	4.79E16±1.58E16bA	2.05E7±5.51E6aA	5.92E10±6.0E9aA	0.08±0.026aA	0.94±0.02
	750	9.23E13±1.95E13bB	1.54E3±2.01E2bC	8.91E29±9.36E28bB	1.11E20±2.89E19bB	4.11E21±9.02E20bB	0.06±0.04abA	0.92±0.02
	1000	5.97E10±5.51E9bA	1.05E3±9.82E1bB	1.75E20±2.99E19bA	3.73E16±7.01E15bA	4.17E17±3.46E16cA	0.15±0.07abA	0.93±0.01

Note: The results are compared by Duncan 's multiple comparisons, different letters on shoulder indicate significant difference among difference moisture content groups (lowercase letters) and difference compression quantity groups (uppercase letter) (P<0.05). The same below.

It can be seen from Table 1 that the coefficients of determination R^2 for fitting the compressive stress-strain curves of CM using the optimized Nishihara model are all greater than 0.92. The results show that the optimized Nishihara model can better describe the compressive mechanical properties of CM.

The elastic modulus reflects the strength of the elastic deformation ability of CM. The larger the value, the weaker the elastic deformation ability and the worse the softness of the inner tissue of CM. In each group of tests in Table 1, E_2 is smaller than E_1, indicating that in the CM compression constitutive model, the elastic deformation capacity of the series spring element E_1 is stronger than that of the spring element E_2 in the Kelvin body, and the flexibility of the former is better than that of the latter.

The viscosity coefficient reflects the strength of CM's anti-deformation viscous resistance. The larger the value, the stronger the anti-deformation viscous resistance and the worse the fluidity of the internal tissue of CM. In each group of tests in Table 1, η_0 and η_2 are close in size, and both are greater than η_1, indicating that in the CM compression constitutive model, the viscous resistance against deformation of the Maxwell body viscous element η_0 and the Coulomb body viscous element η_2 are close, and both stronger than Kelvin body viscous element η_1.

Construct the CM stress relaxation model with the five-component generalized Maxwell model and use the same method to fit and solve the model parameters of CM stress relaxation under different test conditions, namely ε_i, E_a, E_b, η_a, η_b and E_e; then the results were compared and analyzed by the Duncan's method of multiple comparison and are shown in Table 2.

It can be seen from Table 2 that the coefficients of determination R^2 for fitting CM stress relaxation curves using the five-element generalized Maxwell model are all greater than 0.99, and the results show that the optimization of the Nishihara model could describe the mechanical properties of CM stress relaxation.

Through secondary development, the optimized West Proton model, the five-element generalized Maxwell model, and their corresponding parameter values can be applied to software such as ANSYS or ABAQUS to obtain a simulation model that can accurately describe the mechanical properties of CM compression and stress relaxation. Carry out the simulation of CM compression, and dehydration under the operation of different mechanisms, shorten the development cycle of equipment and save the cost of prototype processing.

Table 2

Effects of MC and FL on parameters of CM stress relaxation constitutive model

MC	FM	ε_0	E_a	E_b	η_a	η_b	E_e	R^2
50%	500	0.07±0.02aA	5.36±0.80aAB	1.94±060aA	2.66±1.02aA	34.12±3.32aA	5.86±2.49aA	0.995±0.002
	750	0.04±0.001aA	7.63±0.48aB	2.02±0.48aA	4.32±0.08cA	35.59±1.94bA	9.85±0.21aA	0.996±0.001
	1000	0.067±0.03aA	5.06±1.90aA	1.87±0.29bA	3.16±1.04aA	35.99±1.16bA	7.03±2.332aA	0.995±0.001
65%	500	0.05±0.005aA	9.51±0.43bB	2.02±0.267aA	3.66±0.30aA	30.46±1.13aA	7.37±0.88aA	0.997±0.001
	750	0.07±0.02bA	5.02±1.21bA	2.24±0.38aA	2.52±0.57bA	33.41±1.43bB	5.33±1.14bA	0.996±0.001
	1000	0.07±0.05aA	5.89±2.88aAB	1.99±0.22bA	3.46±1.78aA	34.98±1.31bB	7.07±3.58aA	0.996±0.001
80%	500	0.08±0.044aA	8.70±2.25bB	1.59±0.67aA	2.65±1.14aA	29.86±3.16aA	4.88±2.32aA	0.995±0.003
	750	0.10±0.01cA	5.28±0.62bA	1.48±0.35aA	1.82±0.20aA	30.28±1.20aA	3.42±0.46cA	0.994±0.001
	1000	0.09±0.013aA	5.91±1.02aAB	1.38±0.03aA	2.30±0.38aA	30.23±0.38aA	4.27±0.66aA	0.994±0.001

The influence of various factors on the mechanical characteristics of compression
Moisture content

The influence of MC and FL on the parameters of the CM compression constitutive model was analyzed by using the Duncan mean value comparison method, as shown in Table 1. The results showed that the elastic modulus (E_1, E_2) of different MC groups were significantly different ($P<0.05$). With the increase of MC, the elastic modulus, especially the elastic modulus E_1 in Hooke's body, increased significantly. The reason may be that the hydrophilic group in CM particles absorbs water, making the cell wall stronger and maintaining better elasticity. The difference of viscosity modulus (η_0, η_1, η_2) among groups with different MC was significant ($P<0.05$), which may be due to the positive correlation between viscosity modulus η_0 and MC in CM, the higher the MC, the higher the viscosity modulus, the larger η_0 is. It is comprehensively shown that moisture content and compression quality have a significant influence on elastic modulus and viscous modulus.

Filling mass

Table 1 shows that the elastic moduli (E_1, E_2) of different FM groups were significantly different ($P<0.05$). When MC is 50%, the elastic modulus increases with the increase of FM, probably because the larger the FM, the longer the pressure transmission path, and the local stress generated by the contact and extrusion of CM particles increases, which increases the elastic modulus. When the MC is between 65% and 80%, the elastic modulus first increases and then decreases as the FM increases. The reason may be related to the significant interaction between MC and FM.

The viscous modulus (η_1, η_2) differed significantly among different FM groups ($P<0.05$), which may be due to the fact that FM affects the relative motion between CM particles, resulting in changes in internal friction, which in turn affects the viscous modulus. When MC was 50%, the difference in viscosity modulus η0 was not significant between groups, but the difference in viscosity modulus η0 was significant between 65% MC and 80% MC groups, and the viscosity modulus η_0 increased significantly with the increase of MC. The reason may be that when the MC is 50%, there is less water between the CM particles, the CM is basically in a discrete state, and the viscosity modulus η_0 is not significantly different under different masses.

Influence of various factors on stress relaxation characteristics

Moisture content (MC)

As shown in Table 2, the Duncan mean comparison results showed that the elastic modulus and viscosity attenuation coefficient were significantly different among different MC groups ($P<0.05$), which may be due to the interaction between CM particles and particles and between particles and liquid. Adhesion makes it difficult to disperse during the stress relaxation process, and the change of MC affects the adhesion between CM particles, so there is a significant difference. When FM is 500 g and 1000 g, the elastic modulus and viscous attenuation coefficient change with water content are basically the same between the two groups (basically showing a trend of rising first and then decreasing); when FM is 750 g, elastic modulus and viscous attenuation coefficient increase with water content and reduce. The reasons for the above phenomenon may include both the influence of MC on the adhesion force and the interaction between MC and FM.

Filling Mass (FM)

As shown in Table 2, the Duncan mean comparison results show that the elastic modulus E_a and the viscous attenuation coefficient η_b of different FM groups are significantly different ($P<0.05$), indicating that FM has an effect on the spring element E_a of the first Maxwell body and the spring element E_a of the second Maxwell body. The viscous element η_b has a greater influence. There were no significant differences in elastic modulus E_b, E_e, and viscosity attenuation coefficient η_a among different FM groups ($P>0.05$).

CONCLUSIONS

(1) The uniaxial compression test shows that the compression dehydration process of CM can be divided into three stages: degassing, drainage, and viscoelastic-plastic deformation, and the elastic characteristics are obvious in the early stage and late stages of compression. Multi-parameter fitting the coefficient of determination R^2 is greater than 0.92, indicating that the optimized West Proton model can accurately describe the stress-strain relationship of CM during the compression process.

(2) The results of the stress relaxation test show that the stress decay rate of CM is fast first and then slow, and it only takes 6 s at most for the stress to decay from 0.8 MPa to 0.2 MPa, and the stress decay rate has a negative correlation with FM and MC; The Maxwell model fits the stress relaxation curve of CM, and its coefficient of determination R^2 is greater than 0.99, indicating that the model can fully characterize the stress relaxation characteristics of CM.

(3) The fitting parameters of the CM compression test showed that the elastic modulus and viscous modulus were significantly different among different MC groups ($P<0.05$), and MC and FM had significant effects on the elastic modulus and viscous modulus. The results of stress relaxation fitting parameters showed that there were significant differences in elastic modulus and viscous attenuation coefficient among different MC groups ($P<0.05$). Under different FM, there were differences in the elastic modulus and viscous attenuation coefficient between groups with MC. It may not only include the influence of MC on adhesion but also be related to the interaction between MC and FM.

REFERENCES

[1]　Aguirre-Villegas H. A., Larson R. A., Sharara M. A. (2019), Anaerobic digestion, solid-liquid separation, and drying of dairy manure: measuring constituents and modeling emission. *Science of the Total Environment*, 696, 134059. DOI: 10.1016/j.scitotenv.2019.134059

[2]　Bai Z., Ma L., Jin S., Ma W., Velthof G. L., Oenema O., Liu L., Chadwick D., Zhang F. (2016), Nitrogen, phosphorus, and potassium flows through the manure management chain in China. *Environmental Science & Technology*, 50(24), 13409-13418. DOI: 10.1021/acs.est.6b03348

[3]　Cârdei P., Stefan V., Popa L., Ciupercă R. (2019), Statistical models for the working process carried out by the organic fertilizer spreading machine. *INMATEH Agricultural Engineering*, 58(2). DOI: 10.35633/inmateh-58-13

[4]　Ding Q., Sun H., Li Y., et al. (2023), Establishment and verification of soil mechanical compaction prediction model in paddy field under intensive production conditions (集约化生产条件下稻田土壤机械压实预测模型构建与验证). *Transactions of the Chinese Society of Agricultural Engineering*, 39(3): 42-51. DOI:10.11975/j.issn.1002-6819.202210216

[5]　Ehlers G. A. C., Wagachchi D., Turner S. J. (2012), Nutrient conditions and reactor configuration influence floc size distribution and settling properties. *Water Science and Technology*, 65(1), 156-163. DOI: 10.2166/wst.2011.849

[6]　Guan Z., Xinzhi W., Xu Z., et al. (2016), Optimal design and experiment of screw extrusion solid-liquid separator for cow manure(牛粪污螺旋挤压式固液分离机优化设计与试验). *Transactions of the Chinese Society for Agricultural Machinery*, 47(11): 192-197. DOI:10.6041/j.issn.1000-1298.2016.11.026

[7]　Guilayn F., Jimenez J., Rouez M., Crest M., Patureau D. (2019), Digestate mechanical separation: efficiency profiles based on anaerobic digestion feedstock and equipment choice. *Bioresource Technology*, 274, 180-189. DOI: https://doi.org/10.1016/j.biortech.2018.11.090

[8]　Hjorth M., Christensen K. V., Christensen M. L., Sommer S. G. (2010), Solid—liquid separation of animal slurry in theory and practice. A review. *Agronomy for Sustainable Development*, 30(1), 153-180. DOI: 10.1051/agro/2009010

[9]　Husfeldt A. W., Endres M. I., Salfer J. A., Janni K. A. (2012), Management and characteristics of recycled manure solids used for bedding in Midwest freestall dairy herds. *Journal of Dairy Science*, 95(4), 2195-2203. DOI: 10.3168/jds.2011-5105

[10]　Kong F., Wu T., Chen C., et al. (2021), Mechanical properties and construction of constitutive model for compression and stress relaxation of seed cotton (籽棉压缩与应力松弛力学特性及模型构建). *Transactions of the Chinese Society of Agricultural Engineering*, 37(07): 53-60. DOI:10.11975/j.issn.1002-6819.2021.07.007

[11]　Ma Y., Xuan C., Wu P., et al. (2016), Experiment on stress relaxation of corn stover during compression with assisted vibration (玉米秸秆振动压缩过程的应力松弛试验). *Transactions of the Chinese society of agricultural engineering*, 32(19): 88-94. DOI:10.11975/j.issn.1002-6819.2016.19.012

[12]　Nona K. D., Lenaerts B., Kayacan E., Saeys W. (2014), Bulk compression characteristics of straw and hay. *Biosystems Engineering*, 118, 194-202. DOI: 10.1016/j.biosystemseng.2013.12.005

[13]　Shi H., Lv T., Zhu H., et al. (2014), Rheological properties and apparent viscosity model of pig manure (猪粪流变特性与表观粘度模型研究). *Transactions of the Chinese society for agricultural machinery*, 45(02): 188-193. DOI:10.6041/j.issn.1000-1298.2014.02.031

[14]　Stefan V., Cardei P., Popa L., David L., Ciuperca R. (2019), Influence of the manure spreading machines' working parameters on the qualitative performances of the fertilization process. *INMATEH Agricultural Engineering*, 58(2), 115-120. DOI: 10.35633/inmateh-58-12

[15]　Stefan V., Zaica A., Iosif A. (2021), Research on the uniformity degree of solid organic fertilizers distribution. *INMATEH Agricultural Engineering*, 65(3), 495-504. DOI: 10.35633/inmateh-65-51

[16]　Wang R., Yu J., Wang T., Wang T., Li X. (2021), Experimental study on molding technology for a mixture of corn straw and cow manure. *Bioresources*, 16(1), 1740-1756. DOI: 10.15376/biores.16.1.1740-1756

[17] Wang S., Lv R., Yin X., Feng P., Hu K. (2023), Effects of the ratio of substituting mineral fertilizers with manure nitrogen on soil properties and vegetable yields in China: a meta-analysis. *Plants*, 12(4), 964. DOI: 10.3390/plants12040964

[18] Yao Y., Zhu B., Liu L. (2023), Differential description of basic mechanical properties of different soils (不同类土的基本力学特性差异性描述). *Chinese Journal of Geotechnical Engineering*, 45(1): 33-46. DOI:10.11779/CJGE20220083

[19] Yi X., Yu L., Chang S., Yin C., Wang H., Zhang Z. (2021), The effects of China's organic-substitute-chemical-fertilizer (OSCF) policy on greenhouse vegetable farmers. *Journal of Cleaner Production*, 297, 126677. DOI: https://doi.org/10.1016/j.jclepro.2021.126677

[20] [20] Zhao W., Zhu D., Qu H., et al. (2017), Design and experiment of interrupted-whorl screw extrusion device (断齿式螺旋挤压装置设计与试验). *Journal of Agricultural Mechanization Research*, 39(8): 86-91. DOI:10.3969/j.issn.1003-188X.2017.08.018

[21] [21] Zhao W., Zhu D., Zong W., et al. (2017), Operation parameter optimization of interrupted-whorl screw dewatering device of solid-liquid separator for livestock and poultry manure(畜禽粪污固液分离机断齿螺旋脱水装置运行参数优化). *Transactions of the Chinese society of agricultural engineering*, 33(02): 25-31. DOI:10.11975/j.issn.1002-6819.2017.02.004

[22] Zhu D., Zhao W., Zong W., et al. (2017), Numerical simulation analysis of flow field in flow channel of internal interrupted-whorl screw separator (断齿式挤压脱水流道内流场数值模拟). *Transactions of the Chinese Society for Agricultural Machinery*, 48(10): 92-100. DOI:10.6041/j.issn.1000-1298.2017.10.011